Swarm field-aligned currents during a severe magnetic storm of September 2017

Renata Lukianova[1,2]

[1] Space Research Institute, 117997 Moscow, Russia
[2] Institute of Earth Science, Saint Petersburg State University, 199034 Saint Petersburg, Russia

Correspondence to: Renata Lukianova (renata@aari.nw.ru)

Abstract. *Swarm* satellites observations are used to characterize the extreme behavior of large- and small-scale field-aligned currents (FACs) during the severe magnetic storm of September 2017. Evolution of the current intensities and the equatorward displacement of FACs are analyzed while the satellites cross the pre-midnight, pre-noon, dusk and dawn sectors on both hemispheres. The equatorward boundaries of FACs mainly follow the dynamics of ring current (as monitored in terms of the SYM-H index). The minimum latitude of the FAC boundaries is limited to 50° MLat. The FAC densities are very variable and may increase dramatically, especially on the nightside ionosphere during the storm-time substorms. At the peak of substorm, the average FAC densities reach >3 μA/m^2. The dawn–dusk asymmetry is manifested in the enhanced dusk-side R2 FACs on both hemispheres. Filamentary high-density structures are always observed confirming that a substantial fraction of R1/R2 FACs is composed of many small-scale currents. In the pre-noon sector, the bipolar structures (7.5 km width FACs of opposite polarities adjacent to each other) dominate, while in the post-midnight sector the upward and downward FACs tend to form more latitudinally extended structures of a certain polarity. The most intense small-scale FACs (up to ~80 μA/m^2) is observed just in the post-midnight sector. Simultaneous magnetic and plasma perturbations indicate that this structure is likely a current system of a mesoscale auroral arc.

Keywords: Ionosphere-magntosphere interaction, Field-alighned currents, Storms and substorms, Auroral arcs electrodynamics

1 Introduction

Field-aligned currents (FACs) provide electrodynamic coupling of the solar wind-magnetosphere-ionosphere system. FACs flow along the high-conducting geomagnetic field lines between different magnetospheric domains and the high latitude ionosphere. This current system is driven by the internal magnetospheric circulation of plasma and magnetic field within the global reconnection cycle (Dangey, 1961) and by additional viscous-like interaction at the flanks of magnetosphere (Axford, 1964). Configuration of FACs is primarily controlled by the interplanetary magnetic field (IMF) orientation. Other parameters of the solar wind (velocity, density, IMF strength) and the ionospheric conductivity also play a role (e.g. Christiansen et al., 2002; Ridley 2007; Korth et al., 2002).

Schematic distribution of large-scale FACs has been established by Iijima and Potemra (1976) based on the Triad satellite data. Subsequent space missions allowed constructing comprehensive empirical models of FAC parameterized by the IMF direction and strength, by season, and by hemisphere (Weimer, 2001; Papitashvili et al., 2002; Green at al., 2009). The ionospheric projection of the 3D FAC system consists of a pair of sheets elongated along the auroral oval, namely, Region 1 (R1) and Region 2 (R2), with opposite current flow directions in the morning and evening local time sectors and additional current sheets (R0) located on the dayside poleward of R1/R2. R1 is downward (flows into the ionosphere) and upward (flow from the ionosphere) on the dawn and dusk side, respectively. R1 currents, if reside on closed field lines of the Earth's magnetic field, are believed to originate in either the boundary layer or in the plasma sheet (Ganushkina et al., 2015). R2 FAC is a diversion of the partial ring current to the ionosphere driven by pressure gradients in the inner magnetosphere (Cowley, 2000). R0 current is connected to the dayside magnetopause and its polarity strongly depends on the IMF By component. On the Northern Hemisphere, the R0 current flows predominantly out of the ionosphere for positive IMF By and into the ionosphere for negative IMF By (Iijima et al., 1978; Papitashvili et al., 2002). Additional (NBZ) current associated with the sunward ionospheric flow may appear inside the polar cap, if IMF Bz is northward (Iijima et al., 1984).

While average large-scale current densities typically are of units of $\mu A/m^2$ or less, instantaneous small-scale FACs may reach several hundred $\mu A/m^2$ (Neubert and Christiansen, 2003). The smaller-scale structures are often associated with auroral arcs and ionospheric conductivity and electric field perturbations (Aikio e al., 2002; Juusola et al., 2016). It was shown that in the evening (morning) sector, there is downward FAC equatorward (poleward) of the arc and upward FAC above the arc. The two FAC regions are connected by a poleward (equatorward) horizontal current. Recent studies also confirmed that the cusp plasma injections are accompanied by pairs of FACs, upward at lower latitude and downward at higher latitude (Marchaudon et al., 2006). Significant differences in the characteristics of FACs at different scales, especially near noon and midnight have been found (Gjerloev et al., 2011; Luhr et al., 2015; McGranaghan et al., 2017).

Under stationary conditions the FAC system is evolved in accordance with the reconnection rate, which is controlled primarily by the solar wind. If a substorm occurs, additional FACs form a current wedge

connecting the cross-tail current and the nightside westward ionospheric electrojet (Akasofu, 1964; Lui 1996). The magnitude of existing large-scale FACs also increases (Iijima and Potemra, 1978; Coxon et al., 2014). The dayside R1 currents are found to be stronger than their nightside counterpart during the substorm growth phase, at the same time the R1 oval location moves equatorward. After expansion phase onset, the nightside R1 currents dominate and R1 location moves to higher latitudes (Clausen et al. (2013). Recent studies have also suggested that the substorm current wedge could also include a R2 current system (Ritter and Lühr, 2008).

Magnetic storms are characterized by a dramatic enhancement of energy deposition to the Earth's atmosphere. During a magnetic storm, FACs become highly dynamic because of the enhanced solar-wind-magnetosphere interaction, release of energy stored previously in the magnetotail, particle precipitation and the ring current build up. Storm-time FACs are stronger and more variable compared to stationary FACs predicted by the climatological models. Since the intensity and time evolution of FACs vary from storm to storm, it is of interest to analyze their unique characteristics. Utilizing the magnetic field measurements by *CHAMP* satellite Wang et al. (2006) investigated the northern and southern hemisphere dayside and nightside FAC characteristics during the extreme October and November 2003 magnetic storms. It was shown that as Dst decreases, the FAC region expand equatorward, with the shift of FACs on the dayside controlled by the southward IMF. For both case studies, on the southern (late spring) hemisphere the minimum latitude of the FACs is limited to 50° magnetic latitude (MLat) for large negative values of Bz (The minima are the same, although in October the IMF Bz drops dawn to -28 nT, while in November it reaches -50 nT.) On the northern (late autumn) hemisphere the equatorward boundaries of the FAC region are located at 55-60° MLat. Using the global maps from the *Iridium* constellation Anderson et al. (2005) studied the FACs intensities during severe magnetic storms which occurred during the solar cycle 23 with a particular attention to the evolution of FACs in the course of the storm of August 2000. The results revealed the dawn–dusk asymmetry of the R1/R2 current sheets, with an increase primarily found on the duskside. It was shown that under disturbed conditions the total current is not linearly related to the interplanetary electric field, with the intensity constrained to be below 20 MA (Anderson and Korth, 2007).

Since 2014, comprehensive studies of FAC distributions were carried out based on high precision observations onboard of *Swarm* constellation (e.g. Dunlop et al., 2015; Juusola et al., 2016; McGranaghan et al., 2017). However, the *Swarm* data have not yet been fully utilized for the storm-time FAC analysis. It is the purpose of this paper to characterize the magnitude of the large- and smaller scale FACs as well as their reaction to the magnetic storm development. The *Swarm* observations are used in order to identify various characteristics of the storm-time

FACs for the event of 6–9 September 2017, which was one of the two most severe magnetic storms of the recent solar cycle 24 (the previous event was the St-Patrick storm on 17 March 2015). The September 2017 event is of particular interest because it was a two-step storm during which two major substorms occurred and the FAC system is affected by the storm-substorm interplay. In this paper we investigate the time evolution of the large scale FAC intensities, the displacement of the FAC equatorward boundaries and the extreme small/medium-scale (~7.5 km width) currents.

2 *Swarm* satellites

2.1 Instrumentation

The ESA *Swarm* mission is a constellation consisting of the three identical satellites (hereafter SwA, SwB and SwC, respectively), all are at the low-altitude polar orbit (Friis-Christensen et al., 2008). The *Swarm* constellation was launched in the end of 2013 and enters the operational phase in April 2014. The initial orbit altitude is 465 km (SwA and SwC) and ~520 km (SwB) and the inclination is 87.5°. By September 2017 the orbit altitude decreases down to ~440 and 505 km, respectively. SwA and SwC fly in a tandem separated by 1-1.4° in longitude and the differential delay in orbit is ~3 s. The orbit period is about 93 min and slightly different between SwA/SwC and the upper satellite SwB, so that their along-orbit separation in local time gradually changes. Their orbital planes also gradually drift apart and the separation angle increases by ~20° longitude per year. Slowly drifting in longitude, the orbits cover all the local time sectors over about 130 days.

The mission has a multi-instrument payload. The main module is the high-sensitivity vector (fluxgate type) and scalar magnetometers for determining the magnitude and direction of the total vector and variations of the geomagnetic field with an accuracy of more than 0.5 nT (Merayo et al., 2008). Magnetometers make it possible to carry out measurements in a wide range, including the main magnetic field and the variations of external magnetic field generated by FACs. FACs can be detected by their magnetic perturbations in the orthogonal plane which are obtained after subtracting the Earth's main magnetic field model from the total measured values. From single spacecraft the FAC density can be estimated based on one magnetic component with a techniques invoking Ampere's law under assumptions about the infinite current sheet geometry and the orthogonal crossing of the current sheet. This method was used for the previous one-satellite missions, such as Magsat and Ørsted (Christiansen et al., 2002). It is also applied to each *Swarm* satellite separately. The dual-satellite estimation method

calculates current density from curl(B) measured simultaneously at 4 locations was adapted for SwA and SwC data, where measurements separated along-track will be used to create a 'tetrahedron' (Ritter and Lühr, 2006). The curl(B) method provides more reliable current density estimates, as it does not require any assumptions on current geometry and orientation. The FAC output of both a dual-satellite and a single satellite method are considered to be in a reasonable agreement (Ritter et al., 2013). Both algorithms are implemented in the Level-2 processor to generate the *Swarm* products that are produced automatically by ESA's processing center as soon as all input data are available. The products are provided using the dual-satellite method on the lower pair of satellites SwA and SwC, and the single-satellite solution for each of the Swarm spacecraft individually. The 1 s values of FAC densities are available via the on-line *Swarm* data portal (ftp://swarm-diss.eo.esa.int) as Level 2 data products (Swarm Level 2 Processing System Consortium, 2012). In the present study the single-satellite FACs are used in order to apply the similar method to SwB and SwA/SwC data.

Each Swarm satellite is also equipped with the Electric Field Instrument which includes the Langmuir probe to provide measurements of plasma parameters: electron density, electron temperature and spacecraft potential (Knudsen et al., 2003). These data are available at 2 Hz sampling rate as the standard product of the *Swarm* data base. Combination of the vector magnetometer and the plasma analyzer makes it possible to study the plasma disturbances associated with FACs. The location of the satellite is presented in an geographic coordinate system NEC (*x* North, *y* East, *z* Center), where the *x* and *y* components lie in the horizontal plane, pointing northward and eastward, respectively, and *z* points to the centre of gravity of the Earth. For the purpose of present study all projections of the passes are recalculated to the magnetic local time (MLT) and MLat domain according to coordinate definitions by Laundal and Richmond (2017).

2.2 Orbits on 6-9 September 2017

The polar projection of the satellite orbits as of September 6-9, 2017 on the northern hemisphere is shown in **Fig. 1a**. For mid-September 2017 the projections of the SwB passes are centered in the pre-midnight, pre-noon, dusk and dawn sectors. The successive trajectories (14-15 trajectories per day) are almost parallel to each other and slightly shifted in local time. The satellite SwA (orbits of SwC are very similar) enters the region of MLat>60° between ~09 and 12 MLT, and leave this region between ~21 and 23 MLT. The entry (exit) points of the SwB orbit are located between ~15 and 17 (02 and 04) MLTs. On the southern

hemisphere the direction of the tracks in the MLT-MLat framework is opposite. During a day the orbits is shifted systematically in parallel but, except the near-pole region (MLat>80°), they stay within the early morning, pre-noon, pre-dawn and pre-midnight sectors. The daily variation of MLTs at which the satellites cross the latitude MLat=60° are shown in **Fig. 1b**. The MLT ranges covered by the tracks are presented in **Table 1**.

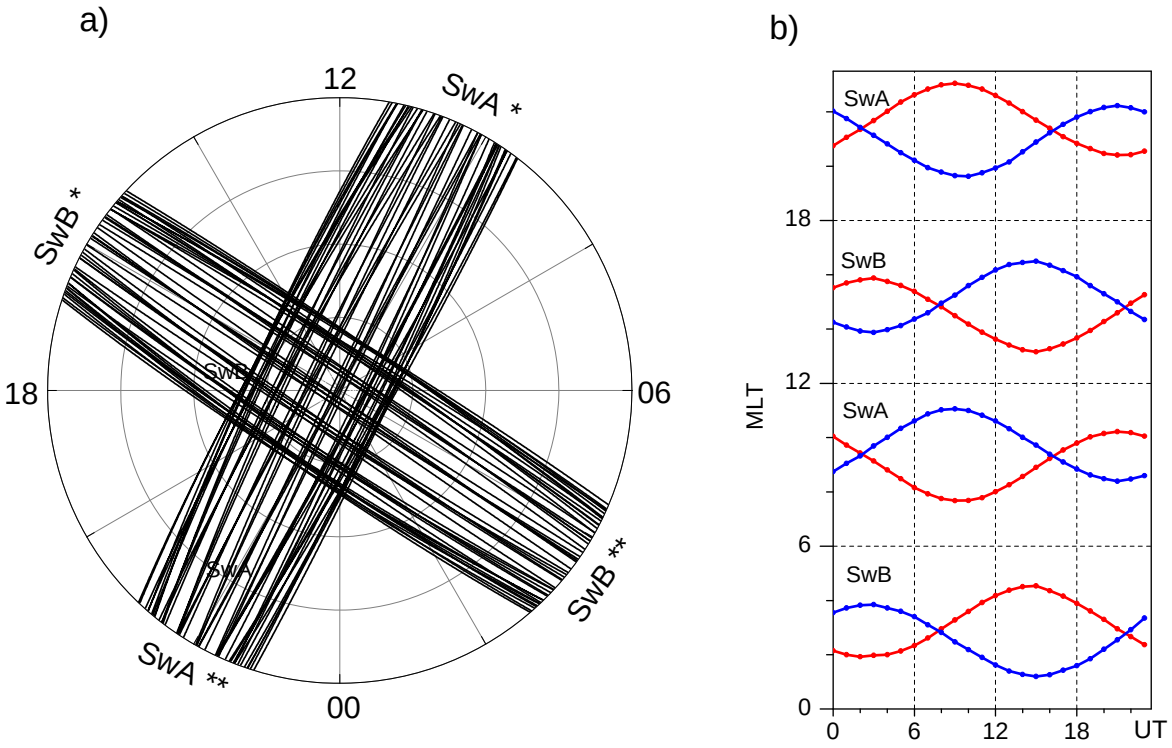

Figure 1: (a) Polar maps of the SwA and SwB orbits on the northern hemispheres on 6-9 September 2017 in the MLT-Mlat framework. Circles are drawn every 10° down to 50° MLat. Symbol * and ** indicates the entry and exit point, respectively. **(b)** Daily variation of MLTs at which SwA and SwB cross the latitude MLat=60° on the northern (blue) and southern (red) hemispheres.

Table 1. Parameters of the tracks in the northern and southern polar regions

Satellite	MLT (hh:mm) ranges within which the satellite cross the boundary of 60° MLat	Center of the MLT range	
		hh:mm	hh
Northern hemisphere			
SwB	02:50-04:40	03:40	04 MLT
SwA (SwC)	09:40-11:30	10:20	10 MLT
SwB	15:00–16:50	16:00	16 MLT
SwA (SwC)	21:10–22:50	22:00	22 MLT
Southern hemisphere			
SwB	03:10-05:00	04:00	04 MLT
SwA (SwC)	09:10-11:00	10:00	10 MLT
SwB	14:50–16:40	15:50	16 MLT
SwA (SwC)	21:20–23:10	22:10	22 MLT

* In the identifier, a letter and a digital symbol denotes the hemisphere and the central hour of MLT, respectively.

3 Space weather conditions on 6–9 September 2017

At the declining phase of solar cycle 24, starting from 6 September 2017, strong multiple solar flares occurred. The associated interplanetary coronal mass ejections collided with Earth's magnetosphere and caused the most intense magnetic storm of the recent solar cycle. The storm produced strong geomagnetic disturbances, ionospheric effects, magnificent auroral displays, elevated hazards to power systems and unstable HF radio wave propagation (Chertok et al., 2018; Clilverd et al., 2018; Curto et al., 2018; Yasyukevich et al., 2018).

Evolution of the SW parameters and geomagnetic activity is presented in **Fig. 2** showing (from top to bottom): the IMF Bz and By, the solar wind proton speed (Vsw) and density (Nsw), the auroral AL and the equatorial SYM-H geomagnetic indices from the OMNI-web service (https://omniweb.gsfc.nasa.gov/). Two SW shock events impact the magnetosphere. The arrival of the first shock late on 6 September (23:50 UT) results in a sudden increase in all parameters except the AL index. Since IMF Bz turns northward, this initial disturbance is only weakly geoeffective as a result. At 20:40 UT on 7 September, IMF Bz turns

southward that triggers a substorm growth phase and a ring current build up. The second shock arrived at ~23:40 UT on 7 September, with the SW speed up to 800 km/s and strongly negative Bz and By. This shock causes an abrupt drop of SYM-H down to -150 nT and a spike-like decrease of AL down to -2200 nT. After 03:00, 8 September the IMF Bz becomes positive, AL gradually approaches to zero and SYM-H starts to recover until the next southward turn of Bz. At ~06 UT on 8 September another strongly negative Bz period is seen, and the SW speed remains high (>700 km/s). This causes the second substorm (AL is -2000 nT) and ring current intensification (SYM-H is -100 nT). A steady recovery occurs in the AL index throughout 9 September, while the SYM-H gradually increases from -75 to -35 nT. The SW parameters are not available for this day.

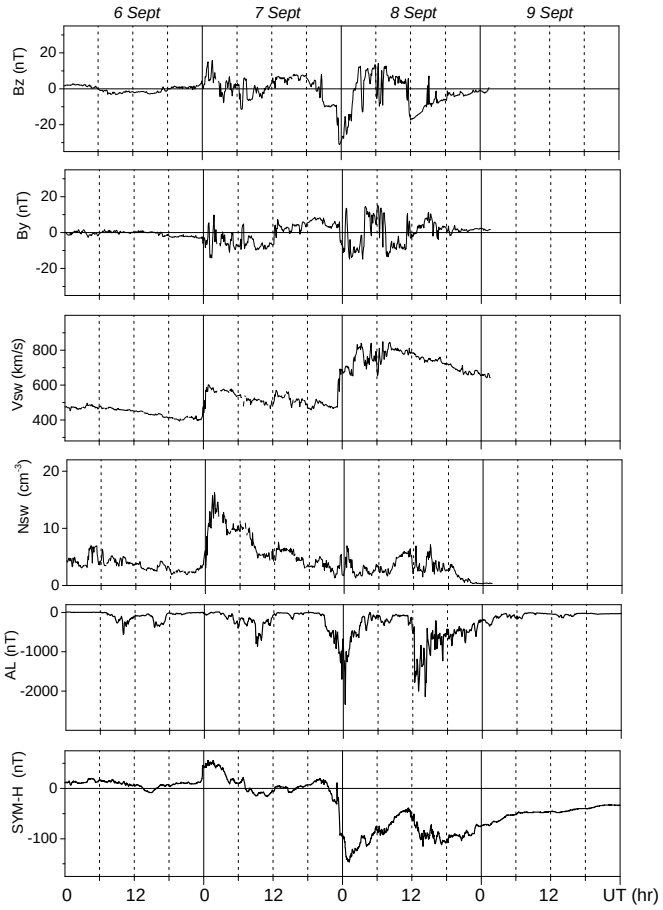

Figure 2: From top to bottom: IMF Bz and By, SW speed and density, AL and SYM-H indices on 6-9 September 2017 (5-min values).

4 Data analysis

4.1 FAC densities

Statistically the large-scale R1 and R2 FAC densities are peaked at the dawn-dusk meridian (Weimer, 2001; Papitashvili et al., 2002; Green at al., 2009). In this regard, satellites orbits on September 2017 are not optimal for identifying the R1/R2 extremes, since they are deviated from this meridian. However, the local time of satellite paths is representative enough to assess the evolution of these FACs. At dusk, the orbits of SwB are centered at about 16 MLT not far from the region, where the current density is expected to be maximal. On the night side, the orbits are centered at 04 MLT, where they overlay the ionospheric westward electrojet. SwA and SwC cross the pre-noon sector at about 10 MLT, where both the downward R1 and upward R2 are often identified. These satellites also cross the pre-midnight sector, where disturbances associated with substorms are expected. An example of the FACs measured along the SwB track is shown in **Fig. 3**.

The 1-s values are presented in **Fig. 3a**, while **Fig.3b** depicts the 21-point smoothed curve from which it can be seen that the satellite approaching the pole from the dusk observes first the downward (positive) R2 and then the upward (negative) R1 current. In the near-pole region (above approximately 72° MLat) FACs are almost absent. Then the satellite move equatorward in the early morning local times. A multi-layer structure is observed, in which the poleward currents are mostly positive, so they may be associated with downward the R1 FAC. The most equatorial currents are negative and thus represent the R2 FAC.

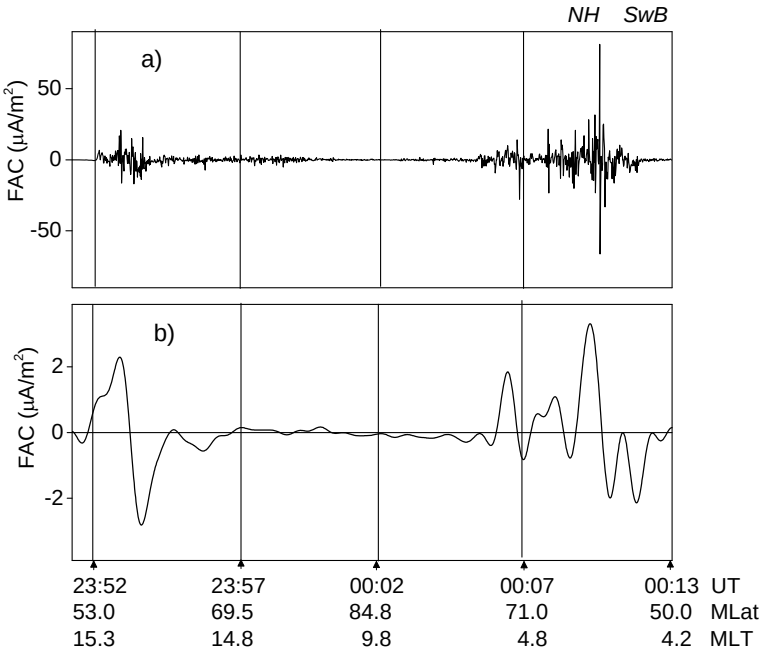

Figure 3: (a) 1 s and **(b)** smoothed FACs measured by SwB in the northern polar region between 23:50 UT, 7 September, and 00:13 UT, 8 September. Downward (upward) current is positive (negative).

To demonstrate the temporal evolution of FACs in **Fig. 4** the FAC intensities for each MLT sector are presented separately for the northern (**Fig. 4a, c, e, g**) and southern (**Fig. 4b, d, f, h**) hemispheres. Red (blue) point is determined by averaging the downward (upward) FAC density from a current-free location at the lowest and highest MLat of each crossing. The upper plots (a-d) and the lower plots (e-h) show the data from day side and night side, respectively. For comparison the evolution of the FAC intensities with the storm development the SYM-H and AL indices are shown in the plots (a, b) and (e, f), respectively. Overall, FACs shown in **Fig. 4,** exhibit three pronounced enhancements, which are of different intensity depending on the MLT sectors. (Note, that the measured FAC densities do not exhibit any systematic changes associated with the daily variation of the orbit.) The first, smaller enhancement in the very beginning of September 7 is seen on the day side (Fig. 4a-d). This increase of FAC intensity is associated with the SW dynamic pressure front impinges the magnetosphere causing a positive excursion of SYM-H. Unlike the day side, on the nightside FACs (Fig. 4e-h) respond to the shock with a considerable delay, so

that FACs are peaked at about 06 UT, 7 September. A moderate substorm occurred in the middle of September 7 also contributes to the increase in FAC intensity.

The two higher peaks occur in the course of the storm main phase at the very beginning and in the middle of September 8. The intensity of a particular peak varies in different MLT sectors being more pronounced on the night side. On the day side, in the sector centered at 10 MLT (Fig. 4a, b) FACs are enhanced during the whole period of 7-8 September with only a relatively modest intensification at about 06 UT on 8 September. In the sector centered at 16 MLT (Fig. 4c, d) an abrupt increase up to 1-2 1 $\mu A/m^2$ is observed at the very beginning of 8 September with association with a first deep drop of SYM-H. On the nigh side, a strong increase of FAC is also observed (Fig. 4e-h). However, the current intensities increase more gradually, although finally they reach the higher values. The nightside FACs follow the evolution of AL and start to increase as the substorm growth phase begins at ~22 UT, September 7. In the sector centered at 04 MLT, northern hemisphere (Fig. 4g) a narrow peak up to 3 $\mu A/m^2$ is observed in the very beginning of 8 September (for a particular crossing the average density exceeds 6 $\mu A/m^2$ as seen from the standard deviation).

The next increase in FACs occurs at ~12 UT on September 8 in association with the second major substorm and the second drop of SYM-H. The corresponding peaks are observed on the night side(the largest average values up to 3 $\mu A/m^2$ are detected on the southern hemisphere (**Fig. 4f, h**), while on the day side the response of FACs to this substorm intensification is weak, if any, although the current densities remain elevated throughout the day. All FACs fall to pre-storm levels by September 9.

Comparison of the evolution of FAC intensity with the SW and geomagnetic parameters during the period of 6-9 September reveals that the storm-time FACs are, on average, by several times larger than the quiet-time ones. Better correlation exists between the night side FACs and the substorm activity (AL index). Although FACs are considerably enhanced during a storm main phase in all MLT sectors, the correlation between the current densities and SYM-H is not strightforward. Also we could not find any simple relation with any isolated SW input, such as the IMF or the SW dynamic pressure.

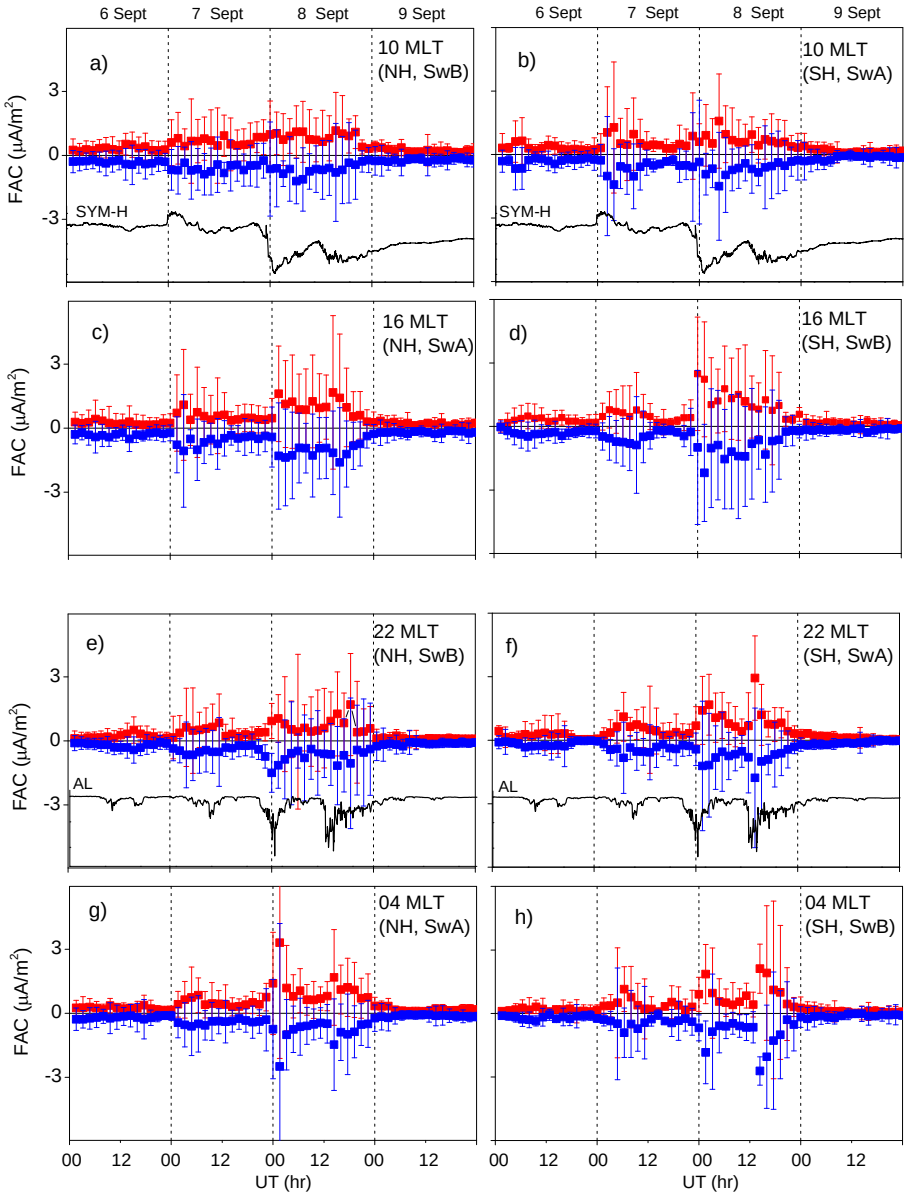

Figure 4: Average FAC densities in the four MLT sectors covered by the *Swarm* data on 6-9 September, 2017. The left column of plots corresponds to the southern (SH) hemisphere and the right corresponds to the northern (NH) hemisphere. The upper plots (a-d) show the dayside data and the lower plots (e-h) show the nightside data. The SYM-H and AL indices are shown in the plots (a,b) and (e, f), respectively. The centered MLT is shown in the right upper corner of each plot. The downward and upward FAC is shown in red and blue, respectively.

4.2 Dawn-dusk asymmetry

During the event of September 2017 a considerable dawn-dusk asymmetry in the storm-time FACs is revealed. Although the estimate is based on a limited number of crossings and does not allow calculating the total FAC, the current densities summed separately over the dawn and dusk sides may serve as a proxy. The sums of the upward/downward FAC densities for the four MLT sectors and for dawn and dusk sides are presented in **Table 2**. All parts of the tracks which fall into the 00-12 MLT (12-00 MLT) sector are considered to be related to the dawn (dusk) side. MLAT for 40°–90° is accounted.

For any given pass, the net summed FAC density is frequently nonzero. As seen in **Table 2 (**columns 3 and 4) the average net FACs summed over the entire 4-day interval in a particular MLT range, is also nonzero. The difference between summed upward and downward current densities varies from 1 to 15%. If the MLT sectors are combined in pairs in order to obtain the currents summed over the dawn and dusk, the prevalence of the dusk-side downward current is revealed. From the FAC values presented in columns 5 and 6 one can see that on both hemispheres the dusk-side downward current is stronger than all the other currents. This predominance implies an additional amplification of the storm-time R2 FAC on the dusk side, which is related to the partial ring current. As pointed out by Anderson and Korth (207) this shift may result from a strong dusk side ion pressure leading to asymmetric dusk-side inflation of the magnetic field consistent with a partial, dusk side, ring current during storm main phase (Liemohn et al., 2001).

Thus the estimation based on the summed FAC densities from the in-situ *Swarm* measurements does indicate the existence of the storm-time dawn-dusk asymmetry. It should be noted that the numbers presented in Table 2 contain uncertainties. Although these numbers are the result of the straightforward summation, there may be indirect factors which lead as to the under- as to the overestimation. For example, the highest MLATs that the satellites reach mayt affect the estimates. However, if the under- as to the overestimation approximately compensate each other, the tendency of the prevalence of the dawn side R2 is revealed.

Table 2. Net summed upward (negative) and downward (positive) FAC densities for all passes on 6-9 September

Side	MLT range (as at 50° MLat)	Summed FAC densities (μA/m^2)			
		up	down	up	down
Northern Hemisphere					
dawn	9.5 – 11.5	-23.3	+23.4	-53.6	+53
	2.9 – 4.5	-31.3	+29.6		
dusk	21.1 – 22.7	-27	+30.1	-52.7	+60
	15.4 – 16.8	-24.7	+29.9		
Southern Hemisphere					
dawn	9.1 - 10.7	-26.8	+27.4	-50.5	+52.7
	3.3 – 4.7	-23.7	+25.3		
dusk	21.1 – 23.2	-23.8	+27.2	-52.5	+58.9
	15.0 – 16.5	-28.7	+31.7		

4.3 Dynamics of the equatorward boundary of the FAC region

It is well established that the enhanced SW input and the pile-up of open magnetic flux during a geomagnetic storm results in the equatorward expansions of the polar cap and the auroral oval as a whole (e.g. Milan et al., 2004). Following the magnetospheric dynamics FACs also move equatorward. **Fig. 5** shows the evolution of the equatorward boundary (EqB) of FACs on 6-9 September. The EqB is determined as the lowest latitude at which FACs are terminated. This latitude is determined using the 21-point sliding window moving along a track. The procedure applied to the 1 s data according to the following criterion: at least eight values before and after the central point do not exceed 0.1 μA/m^2. If the criterion is fulfilled, the most poleward point without FAC is selected as EqB. Than the results are checked visually in order to avoid the erroneously calculated latitudes, that may happen, e.g., if a latitudinal gap between R1 and R2 occur. When calculating EqB, no separation between the up- and downward large-scale FACs has been made.

Even visual comparison of the SYM-H and EqB evolutions reveals a coherent behavior of these two parameters. At the same time, during a period preceding the storm main phase (before end of 7 September, when SYM-H is mainly positive) EqB is located much lower than during the end of recovery phase (after ~12 UT on 9 September, when SYM-H is still negative). From **Fig. 5** one can see that during the pre-storm time (before the SYM-H attains its stable negative values <-20 nT at 22:00 on 7 September) FACs are observed mainly poleward of 60° MLat on both hemispheres. Moderate equatorward shifts of EqB are associated with the modest substorms occurred before the storm main phase in the middle of 6 and 7 September. Prior the storm main phase, on both hemispheres the prenoon (04 MLT) EqB is found considerably poleward compared to the EqB location at other MLTs. The effect is well seen during the two time intervals: from ~22 UT, Sept 6 till 06 UT, Sept 7 and after 12 UT, Sept 7. Both intervals are dominated by the northward IMF (sf. **Fig. 2**), so that a shrinking of the polar cap and a poleward shift of the auroral oval is expected. With regard to the position of FACs, the displacement of its equatorward boundary is the largest only in the pre-noon sector, while the other local times remain less affected.

Upon arrival of the SW shock at the very end of September 7, EqB is shifted equatorward, then tends to recover, and then drops again following the second intensification of the storm. At the very beginning of 8 September EqB is found at its lowest position at 50° MLat. The EqB drops abruptly and simultaneously with the peak of the first storm-time substorm just between 7 and 8 September and with the lowest drop of SYM-H down to -150 nT. The second substorm reaches its peak slightly before the second minimum of SYM-H (at 12:50 and 13:55, respectively). During the second activation of the storm the EqB is shifted again as low as 50° MLat (although SYM-H is only -100 nT). As seen from **Fig. 5**, the evolution of EqB tends to follow the gradual change of SYM-H rather than an abrupt drops of AL related to the substorm onset (see also **Fig. 2** for AL). Unlike the current density, which exhibits sharp spike-like increases, temporal variations of EqB are relatively smooth. During the late recovery phase at the second part of September 9, EqB is shifted poleward as high as 70° MLat. As far as the day-night asymmetry is concerned, almost no notable difference in evolution on the day- and nightside EqBs is observed during the main and recovery phases. An expansion of the FAC region during the substorm growth phase, and then a contraction are not resolved.

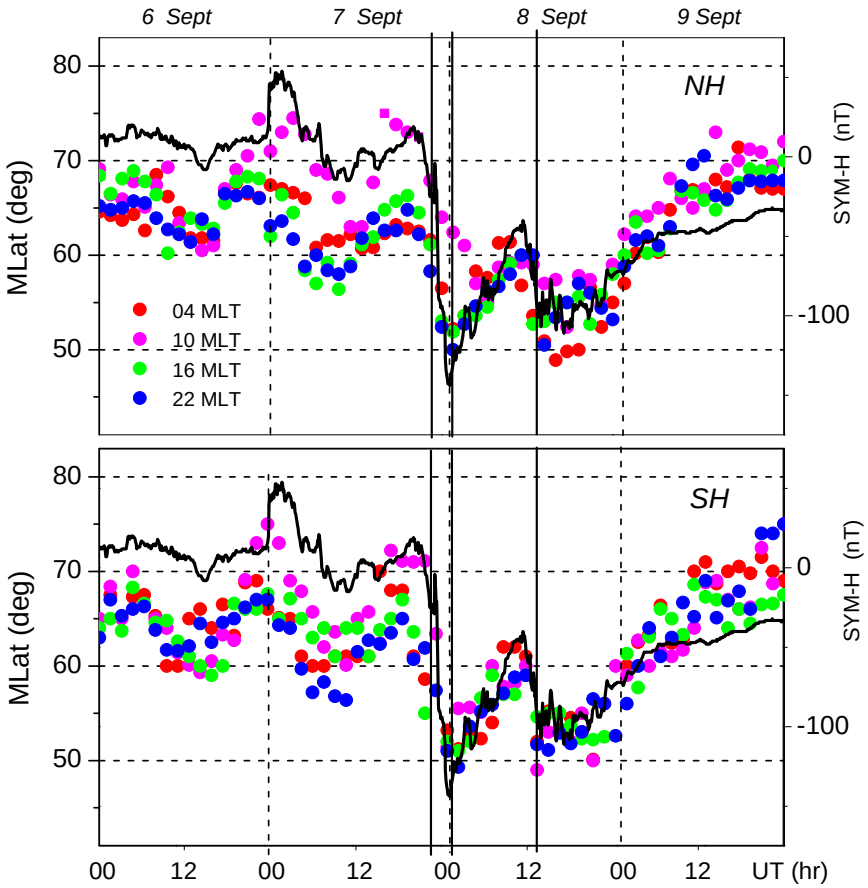

Figure 5: Magnetic latitude of the FAC equatorward boundaries on the northern (top) and southern (bottom) hemispheres for four MLT sectors centered at approximately 04, 10, 16 and 22 MLT (see **Table 1**) on 6-9 September 2017. The SYM-H index is shown by black line in each plot. Three vertical solid lines mark successively the beginning of the storm main phase at 22:00 on 7 September (the time when SYM-H attains its stable negative values <-20 nT), the peaks of the first and second major substoms (the time when AL attains its minimum)

4.4 Small-scale FACs

FACs appear on a wide range of scales from large-scale sheet-like currents of hundreds kilometers width to very small-scale filamentary currents of hundreds meters width. The current intensity vary inversely with scale so that large-scale currents are typically a few μA/m^2, whereas the smaller scale (down to 10 km) are

a few tens μA/m^2 (Neubert and Christiansen, 2003; McGranaghan et al., 2017). The standard *Swarm* time-series provide the spatial resolvution of ~7.5 km. The quasi-instantaneous amplitudes of these small scale component of FACs are often much larger than the stationary R1/R2 FACs. To obtain the time-series of peak current densities, the largest positive and negative 1 s values were selected from each crossing of a given MLT time sector irrespective of the hemisphere. The time-series of peak values are presented in **Fig. 6**. From the figure one can see that the small-scale peaks may be more than an order of magnitude larger than the FACs averaged over a track. During the disturbed period, starting with the compression of the magnetosphere on September 7, the amplitude of FACs tends to increase. Two intense substorms occurring during the storm main phase are accompanied by an additional strengthening of small-scale FACs. Both the up- and downward currents strengthen with increased geomagnetic activity and attain their extremes of ~80 μA/m^2) near the midnight between September 7 and 8.

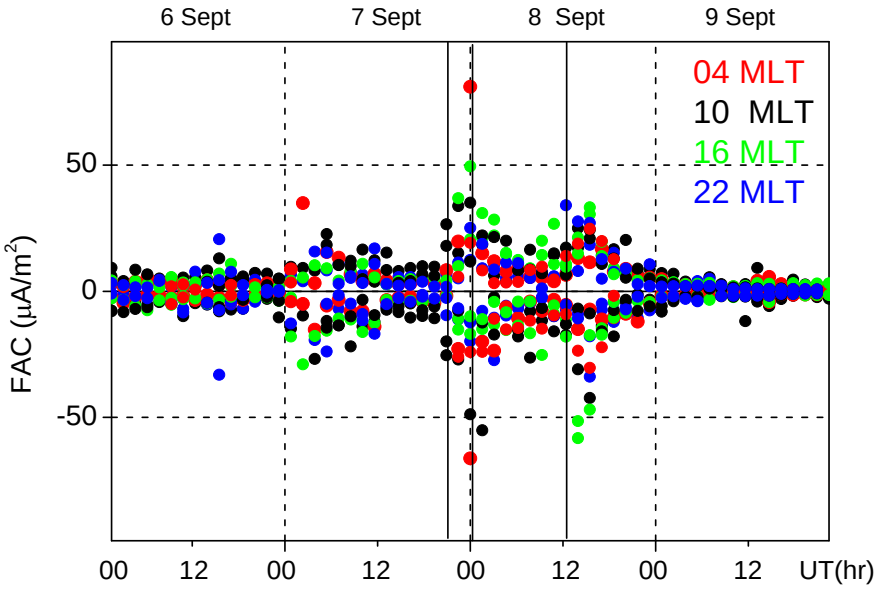

Figure 6: The largest downward (positive) and upward (negative) 1 s current densities for four MLT sectors on 6-9 September. Three vertical solid lines mark successively the beginning of the storm main phase at 22:00 on 7 September (the time when SYM-H attains its stable negative values <-20 nT), the peaks of the first and second major substoms (the time when AL attains its minimum)

When for each crossing of the region of MLat>50° within a certain MLT sector the minimum (i.e. the peak upward current) and maximum (i.e. the peak downward current) of 1 s FACs were selected, it appears that in some cases the adjacent upward and downward currents (called hereafter the bipolar structure) are observed, while in other cases the min/max are separated in latitude. In **Fig. 7**, the correlations between the MLats, at which the most intense small-scale FACs of opposite polarities are observed, are presented separately for the four MLT sectors. The x-axis (y-axis) corresponds to the MLat at which the downward (upward) 1 s FAC is observed. It is seen that in the pre-noon sector (**Fig. 7b**) the correlation between the latitudinal positions of the up- and downward FACs is high (the correlation coefficient is 0.94). This is indicative of a large population of the paired, closely adjacent small-scale currents of opposite polarity. In the post-noon sector (**Fig. 7a**) the correlation coefficient decreases down to 0.78. Slightly weaker correlation (cc=0.75) is observed in the pre-midnight sector (**Fig. 7c**). At the early morning hours (**Fig. 7d**) the correlation is poor (cc=0.53). Despite some spatiotemporal ambiguity inherent in single satellite observations, it can be speculated that in the early morning local time sector the up- and downward currents appear less frequently in pair but rather are separated by a distance greater than 8 km.

In contrast to the early morning local times, in the pre-noon sector, where cusp and cleft currents are expected, the bipolar structures are quite frequent. Here, these structures may represent a signature of the cusp plasma injections which are accompanied by pairs of FACs generated due to flux transfer event (FTE) formation (Southwood, 1987) or localised reconnection at the magnetopause. Magnetic topologies associated with FTEs were previously observed by the MEO satellites (Marchaudon et al., 2004; 2006; Pu et al., 2013) but not by the LEO satellites. Neubert and Christiansen (2003) reported small-scale currents primarily found in the cusp and pre-noon region with densities 1–2 orders of magnitude larger than R1 and R2 currents. The dependence on IMF Bz and the SW turbulence was found by these authors suggesting that currents are a result of reconnection processes distributed over the dayside magnetopause and even in the tail for negative Bz. The bipolar structures were not resolved in the observations by Neubert and Christiansen (2003). The correlations presented in **Fig. 7** may be interpreted in such a way that the bipolar structures dominate exactly in the region where the signatures of FTE and the multiple reconnection lines formed at the magnetopause are expected.

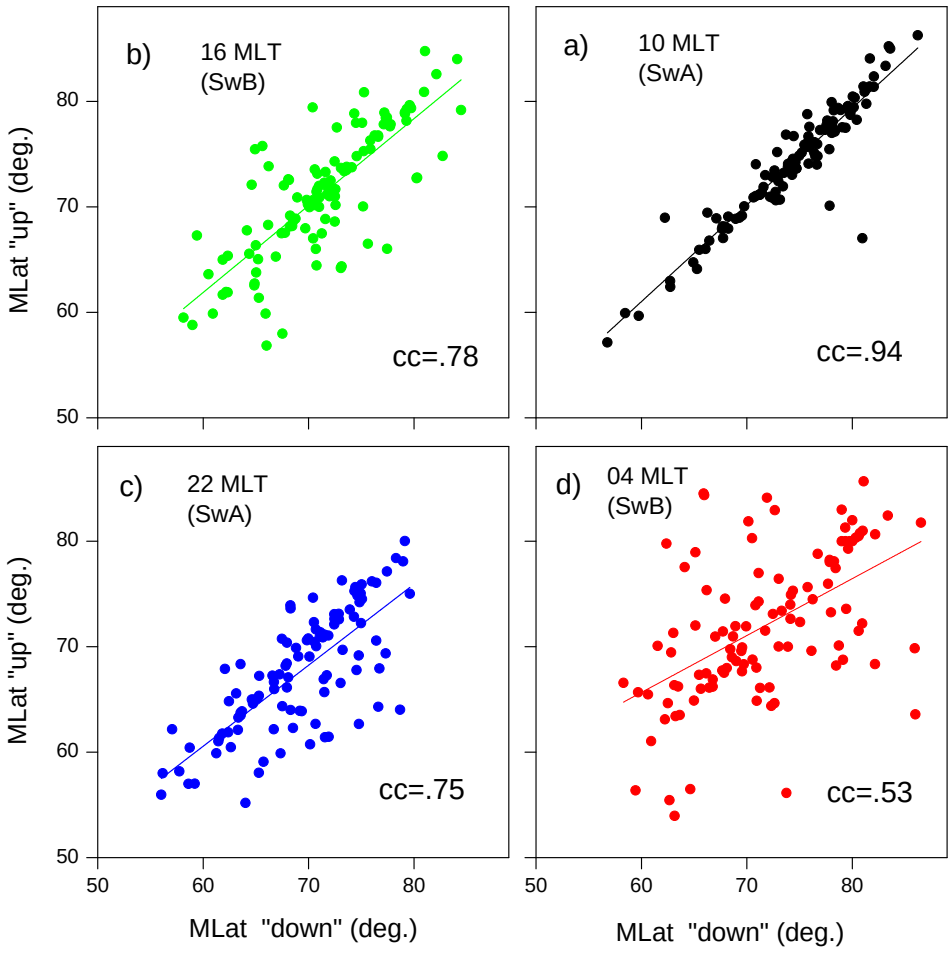

Figure 7: Correlations between MLats, at which the up- and downward FACs are observed in the four MLT sectors: **(a)** post-noon/dusk, **(b)** pre-noon, **(c)** pre-midnight, **(d)** post-midnight.

4.5 Small-scale FACs of extreme amplitude

A pair of the most intense upward and downward small-scale FACs is observed by SwB when the satellite traverses the latitudinal range of 60-80° MLat from north to south over the geographic area of the Barents

Sea. The 1 s FACs and plasma parameters (the electron density, Ne and temperature, Te, and the spacecraft electric potential, U_{sc}) measured by SwB for a period of 00:08:00-00:12:00 UT on 8 September during the growth phase of the first storm-time substorm are shown in **Fig. 8**. The original current densities are superimposed to the smoothed curve, which reveals a multi-layer structure with several large-scale upward and downward FACs (**Fig. 8a**). Among them, the strongest (up to 30 μA/m^2) is the downward R1 FAC located at ~62° MLat. At 00:10:18 and 00:10:19 UT (latitudinally in between the downward R1 and upward R2 FACs) the satellite observes a pair of downward (81 μA/m^2) and upward (-66 μA/m^2) peaks. These paired small-scale up- and downward FACs of comparable values form a bipolar structure in which the currents are balanced and likely closed locally.

This current structure is accompanied by an increase in Ne. A narrow peak in Ne up to $77 \cdot 10^3$ cm^{-3} (**Fig. 8b**) and an increase of Te up to about 10^4 K on average (**Fig. 8c**), that is ~50% above their ambient values, are observed at 00:10:23 UT. It should be noted that the Te values presented here are based on the current processing of the satellite data and may be still uncalibrated. However, it hardly affects the relatively small-scale perturbations. Elevations of Te are observed in a wider region slightly poleward of the enhanced Ne. The plasma disturbances are clearly seen in U_{sc}, which is proportional to $-k \cdot Te$ (k is the Boltzmann constant). Note, the level of noise for the U_{sc} channel is much lower compared to that for the Te channel (0.4% and 2% for U_{sc} and Te, respectively). **Fig. 8d** shows a reduction of U_{sc} started at 00:09:56 UT and peaked at 00:10:08 (-12 V) and at 00:10:20 UT (-8 V), the average decrease is -5 V. The width of the region of the Te and U_{sc} perturbations is several times the width of the pair of extreme FACs and Ne. The localized increase of Ne and consequent conductance enhancement are likely due to precipitating electrons. The observed plasma and current perturbations are similar to those associated with auroral arcs (Opgenoorth et al. 1990; Lyons, 1992; Lewis et al., 1994; Johnson et al., 1998; Aikio et al., 1993; Juusola, et al., 2016). In particular, Aikio et al. (2002) studied the current system of arcs in the evening sector, where the background electric field is northward. It was shown that for arcs located within the northward convection electric field currents flow downward on the equatorward side of the arcs, then poleward, and upward from the arcs. The arcs are associated with an enhanced northward-directed electric field region on the equatorward side of the arc. An enhancement in the electric field starts already several tens km equatorward of the arc edge.

During the storm under consideration the bipolar FAC pattern observed at 00:10 UT is located in the morning sector, where the background electric field is expected to be southward. This is confirmed by the SuperDARN-based convection model (http://vt.superdarn.org/tiki-index.php?page=ASCIIData), which predicts in the region of the SwB observations the magnitude of the southward and westward component of about 6.5 mV/m and 0.5 mV/m, respectively. For morning side arcs an enhanced southward electric field on the poleward side of the arc is expected. In this case the current pattern consists of a downward FAC on the poleward side of the arc connected to an upward current above the arc by an equatorward ionospheric closure current. This is exactly what is seen in **Fig. 8a**: when SwB flies away the pole, it first observes a positive spike (downward FAC) and then a negative spike (upward FAC). Since the width of the region of enhanced Ne is ~30 km, the arc is relatively narrow. Comparing **Fig. 8a** and **Fig. 8b** one can see that the paired FACs is located on the poleward side of the region of enhanced Ne. Note, that in **Fig. 8b** a sharp increase in Ne up to ~80 $\cdot 10^3$ cm^{-3} is preceded by a weaker spike-like drop down to ~30 $\cdot 10^3$ cm^{-3}. A decrease in Ne (which is usually much less pronounced than an increase due to precipitating electrons) is associated with a downward FAC observed at the opposite boundary of the arc. Elevations of Te may be created by electric fields which can arise within narrow region adjacent to the northern side of the auroral arc as observed by Aikio et al. (2002).

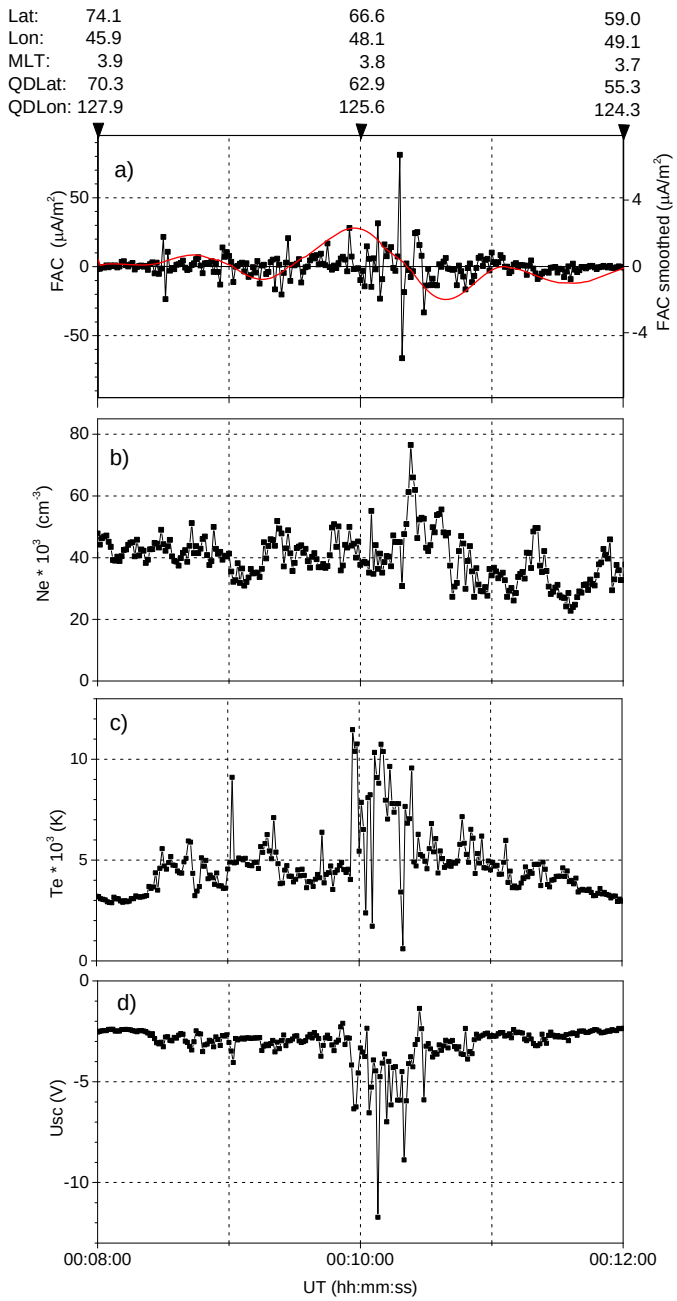

Figure 8: The 1 s values of **(a)** FAC density, **(b)** Ne, **(c)** Te, and **(d)** Usc measured along the SwB track at 00:08:00 – 00:12:00 UT, 8 September. In the upper plot the 21-point smoothed FAC density is also shown. Geographic and geomagnetic coordinates are shown on the top.

5 Discussion

Observations of the LEO *Swarm* multi-satellite mission are used in order to identify various characteristics of the storm-time FACs for the severe event of 6–9 September 2017. During the storm main phase two major substorms occurred, so that the FAC system evolved under conditions of the storm-substorm interplay. In mid-September 2017 the separation between the upper and lower *Swarm* satellites was about 6 hours in local time. Within the sectors centered at 04, 10, 16 and 22 MLT T\the northern and southern polar regions were covered by about 60 tracks along which the 1 Hz measurements of FACs were carried out. These observations made it possible to reveal the evolution of the large scale FAC intensities, the displacement of the FAC equatorward boundaries and the some features of the extreme small/medium-scale (~7.5 km width) FACs.

5.1 Large-scale FACs

Evolution of large-scale FACs during the September 2017 storm is in general agreement with regularities observed previously by *CHAMP* during the intense 2003 geomagnetic storms (Wang et al., 2006). The common feature of all storm-times is the equatorward motion of FACs correlating with the storm intensity as monitored in terms of the SYM-H index. At the same time, some notable features are found for the September 2017 storm. In all four MLT sectors the FAC intensity was enhanced starting from the time of the first SW shock arrival at the very beginning of 7 September despite of the northward IMF and the prolonged period of geomagnetic quietness. After approximately a day, a magnetic storm abruptly commenced at ~22: UT on 7 September. During the two-step main phase of the storm FACs exhibit three pronounced enhancements, which are of different intensity depending on the MLT sectors. On the dayside FACs strengthen mainly in response of the first drop of SYM-H, while the response to the second drop of SYM-H is relatively weak. On the night side the current intensities follow mainly the substorm dynamics as monitored in terms of the AL index. During the period between the substorms, when the AL index is recovered, FACs stay considerably enhanced. Clausen et al. (2013) utilized the data from the Advanced Magnetosphere and Planetary Electrodynamics Response Experiment (AMPERE) to study temporal and spatial dynamics of the R1/R2 currents during isolated substorms. It was shown that the dayside R1 currents are stronger than their nightside counterpart during the substorm growth phase, whereas after

expansion phase onset, the nightside R1 currents dominate. For the second storm-time substorm occurred on 8 September the Swarm observations are in agreement with this regularity. The response of the FAC intensities to the first storm-time substorm is seemed to develop rapidly and the dayside FACs do not exceed the nightside FACs during the growth phase. The effect is likely related to a large amount of energy entered to the magnetosphere from the solar wind due to the viscous-like interaction even if the IMF is northward.

The September 2017 storm is characteristics of a considerable equatorward expansion of the FACs region. For the 2003 storms, the minimum latitude of peak current density are limited to 52-56° MLat (Wang et al., 2006), while for the 2017 storm the EqB expand as low as 50° MLat on both hemispheres. It should be noted that Wang et al. (2006) defined the latitudinal positions of peak current density but not the most equatoward boundary of the FAC region. Thus the actual FAC region in 2003 may expand to lower latitudes. In 2017 the latitudinal positions of EqB generally follow the SYM-H index variation. Despite the 2017 storm is considerably weaker (Dst≈-100 nT) than the 2003 storms (Dst≈-400 nT), in the 2017 event, the FACs are found at approximately the same latitudes. This effect may be interpreted in terms of saturation, when the FAC region does not expand lower than about 50° MLat independent of the storm severity.

Linear dependence between latitudinal boundaries of the FAC sheets upon the dayside merging electric field, the AE and Dst indices has been reported by Xiong et al. (2014). It was pointed out that toward high activity a saturation of equatorwards expansion seems to set in. In accordance with these results, in 2017, the FAC boundaries primarily respond to the storm development, which is mainly governed by the IMF Bz turning southward. Also, FACs are shifted further equatorward during the storm-time substorms. Even a relatively minor substorm occurred prior the storm causes an equatorward displacement of FACs. The lowest latitude of EqB is observed when both the SYM-H and AL indices reach their minimums.

In 2017, in the course of the storm main phase no considerable difference between the latitudinal positions of EqB in different MLT sectors is observed. After ~12 UT on September 9, the day- and nightside EqBs recover to undisturbed position (about 70° MLat), although the storm recovery phase continues (SYM-H ≈ -50 nT). Previous analysis of the latitudinal shift of the polar cap boundaries based on the *IMAGE*

observations during a magnetic storm has shown that, if the IMF Bz turns northward, the dayside boundary recovers much faster than the nightside boundary (Lukianova and Kozlovsky, 2013). In the *Swarm* data the poleward boundaries of the FAC region are not clearly identified. However, it seems that the nightside EqB recovery does not exhibit any delay compared to the dayside EqB. Prior the storm main phase, when the IMF Bz is northward, the pre-noon EqB is located at higher latitudes (~75° MLat) compared to the other MLT sectors (~65 MLat). Determination of the poleward FAC boundary is less reliable than determination of the equatorward one. It is because in some cases (if the satellite does not traverse the central polar cap) the FACs are observed during the entire crossing of the polar region, so it is not possible to construct a continuous time series of the polar latitudes at which FACs are terminated.

Evolution of FAC densities only generally follows the same tendencies as the latitudinal position of EqB. In particular, the latitudinal displacement of FACs is more gradual and smooth compared to the changes in current intensity. The FAC densities, especially on the night side, promptly respond to the onset of storm-time substorms. The fact that the R1/R2 current intensity is controlled most efficiently by substorm evolution was pointed out by He et al. (2014). Comparing the evolution of the FAC densities and the equatorial boundary positions during the storm recovery, one can see that the densities decay much faster than the boundaries return to their quiet time positions.

The *Swarm* observations are in accordance with the previously observed dawn-dusk asymmetry in the FAC distribution. While the summed FAC intensities are comparable between the two hemispheres, the positive and negative densities in a certain MLT sector are slightly imbalanced and the net current is nonzero. The dawn-dusk asymmetry is revealed by comparing the up- and downward FACs, which are summed separately over dusk and dawn. The largest values are characteristics of the dusk-side downward R2 FACs. The observed imbalance in FACs is likely related to an intensification of partial ring current (PRC), which is connected to R2 FAC. Strengthening of PRC may also lead to asymmetric dusk-side inflation of the geomagnetic field lines. The asymmetry in the equatorward displacement of R1 and R2 at the peak of the major storm on August, 2000, has been reported by Anderson and Korth (2007). For the storm of September 2017 almost no difference in the equatorward shift of the dusk and dawn side FACs is observed. During this particular storm the dawn–dusk asymmetry is rather manifested in the enhanced density of R2 FAC on the dusk side.

5.2 Small-scale FACs

Due to their large amplitudes medium and small-scale FACs play an important role for the energy input to the upper atmosphere. In several previous studies, the FACs associated with arcs were estimated as 1-10 μA/m^2 (Bythrow and Potemra, 1987; Elphic et al., 1998; Janhunen et al., 2000). Larger range of current densities, varying between 4 and >40 μA/m^2, has been observed (Aikio et al., 2002) and even more intense small-scale FACs, up to hundred of μA/m^2, at the edges of arcs have been measured (Marklund et al. 1982; Bythrow et al. 1984). Such a large range of the FACs estimates is likely related to its different scales, because for arcs with very sharp electron density gradients, the FACs associated with ionospheric currents flow in narrow regions at arc edges. If the real widths are smaller, the current densities will be larger.

During the September 2017 magnetic storm one of the *Swarm* satellites managed to observe a pair of the most intense small-scale FACs of opposite polarity, the magnitude of which are approximately +80 and -70 μA/m^2. These up- and downward FACs are separated in a fraction of degree in MLat. The FACs occur just prior of the substorm onset and they located in the region between R1 and R2 in the vicinity of the newly developed ionospheric WEJ. The polarity reversal captured by the *Swarm* data for two consecutive seconds implies a quite localized current closure through the ionosphere mostly via Pedersen horizontal currents. Although without optical data one could not make a strict conclusion, the small-scale bipolar FAC pattern accompanied by a localized enhancements in Ne and Te are likely associated with mesoscale discrete aurora. One-to-one correspondence of small-scale FACs with localized electron precipitation events has been previously observed (Fukunishi et. al., 1991).

The considerably elevated Te within the arc and just poleward of the arc is likely associated with a local amplification of electric field (the Swarm electric field data are inavailable). Meanwhile, the SwB observations are in agreement with the disturbances expected for the acrs occurred on the morning side, where the ambient electric field is southward. The observed features are resemble to those reported by Aikio et al. (2002) but bearing in mind that the latter are related to the evening sector, where the background electric field is northward.

Based on *Swarm*/*THEMIS* ASI observations Wu et al. (2017) has associated multiple auroral arcs with up/down current pairs. For these arcs unipolar and multipolar FAC systems with current densities of about

a few μA/m^2 have been observed. Arcs in unipolar FAC systems have a typical width of 10–20 km and a spacing of 25–50 km. Arcs in multipolar systems are wider and more separated. In the bipolar structure observed by SwB during the September 8 event, the current density exceeds the density observed by Wu et al. (2017) at least by a factor of ten, while the spatial extend of FACs is smaller. This difference implies the existence of sharp electron density gradients at arc edges.

Filamentary high-density structures are always presented in the *Swarm* observations. This implies that a substantial fraction of R1/R2 currents is composed of many small-scale FACs. The narrow high-density currents are averaged out when integrated over a FAC region, so that multilayer structures of steady large-scale FACs depicted by Iijima and Potemra (1978) can be revealed after a proper smoothing. From a statistical study of the temporal and spatial-scale characteristics of different FAC types derived with the *Swarm* satellites Luhr et al. (2015) have shown that small-scale, up to some 10 km FACs are carried predominantly by kinetic Alfven waves. A persistent period of small-scale FACs of order 10 s, while large-scale FACs can be regarded stationary for more than 1 min. Neubert and Christiansen (2003) studied the morphology of very small-scale FACs from a survey of *Oersted* satellite 25 Hz data. These FACs are distributed in a broad region around the pre-noon and cusp region, and in the pre-midnight sector. It was found that at the considered time scale, instantaneous currents may reach the largest values up to 1000 μA/m^2, while the average current densities reach a maximum of 10 μA/m^2. McGranaghan et al. (2017) demonstrated a local time dependence in the relationships between large (>250 km) and small FAC scales (10–150 km width, density is up to 0.5 μA/m^2). It was found that linear relationships exist near dawn and dusk local times, while at noon and midnight local times no similar regularity is seen. The results are based at all available data from the *Swarm* satellites and the AMPERE irrespective of the level of geomagnetic activity.

6 Conclusion

Characteristics of FACs inferred from the *Swarm* observations during the severe magnetic storm of 6-9 September 2017 are presented. This storm is the two-step one and the intense substorms occur in the course of the storm main phase. The satellites cross the pre-midnight, pre-noon, pre-dusk and pre-midnight sectors. The following features of the storm-time FACs are found.

Evolution of the current intensities and the latitudinal position of the equatorward boundaries of the FAC region are controlled by a storm-substorm interplay. The FACs become enhanced starting from the SW shock arrival despite of the prolonged period of the northward IMF. The night-time FAC densities primarily follow the substorm development while the dayside FACs are intensified primarily in response to the SW shock. At the peak of substorm, the FAC densities averaged over a track within a given MLT sector, reach 3 $\mu A/m^2$, while the undisturbed level is about 0.2 $\mu A/m^2$. The dawn–dusk asymmetry is manifested on the enhanced dusk side (downward) R2 FAC on both hemispheres.

The equatorward displacement of FAC sheets (in the north and south and at all MLTs) correlates with the storm intensity as monitored by the SYM-H index. The minimum latitude of the equatorial FAC boundaries is limited to 50° MLat. Displacement of FAC sheets is more gradual and occurs with a considerable time delay compared to the changes in current intensity.

The small-scale filamentary structures of high-density FACs are always presented in the *Swarm* observations. A bipolar structure of FACs (up to ~80 $\mu A/m^2$, 7.5 km width) of opposite polarities is observed in the vicinity of the newly developed WEJ just prior of the substorm onset. Simultaneous plasma perturbations indicate that the bipolar FAC pattern is likely associated with mesoscale auroral arc. For the extremes of the small scale FACs the bipolar structures (i.e. the adjacent upward and downward currents) are quite frequent in the pre-noon sector, that may be a signature of the cusp plasma injections.

Data availability: The data used for the publication of this research are freely available from the *Swarm* Science Team web site (ftp://swarm-diss.eo.esa.int). Data selected for the analysis are available upon request (RL).

Competing interests: The author declare that she has no conflict of interest concerning this paper.

Acknowledgement

Swarm data are available through the European Space Agency Online platform (ftp://swarm-diss.eo.esa.int), after registration. We acknowledge the *Swarm* Science Team for providing the level 2 data and the *Swarm* visualization tool (https://vires.services/). The OMNI data on the solar wind, interplanetary magnetic field and geomagnetic indices are obtained from NASA/GSFC's Space Physics Data Facility's CDAweb service (http://omniweb.gsfc.nasa.gov/). This research was partly supported by the RFBR (grant 17-05-00475).

References

Aikio, A.T., Opgenoorth, H.J., Persson, M.A.L., and Kaila, K.U.: Ground based measurements of an arc-associated electric field, J. Atmos. Terr. Phys., 55, 797–808, 1993.

Aikio, A.T., T. Lakkala, A. Kozlovsky, and Williams, P.J.S.: Electric fields and currents of stable drifting auroral arcs in the evening sector, J. Geophys. Res., 107(A12), 1424, doi:10.1029/2001JA009172, 2002.

Akasofu, S.-I.: The development of the auroral substorm, Planet. Space Sci., 12, 273–282, 1964.

Anderson, B. J., S.-I. Ohtani, H. Korth, and A. Ukhorskiy, Storm time dawn-dusk asymmetry of the large-scale Birkeland currents, J. Geophys. Res., 110, A12220, doi:10.1029/2005JA011246, 2005.

Anderson, B.J., and Korth, H.: Saturation of global field aligned currents observed during storms by the Iridium satellite constellation, J. Atmos. Solar-Terr. Phys., 69, 166–169, 2007.

Axford W.I., Viscous interaction between the solar wind and the Earth's magnetosphere. Planet. Space Sci.12 ,45, 1964.

Bythrow, P.F., and Potemra, T.A.: Birkeland currents and energetic particles associated with optical auroral signatures of a westward traveling surge, J. Geophys. Res., 92, 8691–8699, 1987.

Chertok, I.M., Belov, A.V., and Abunin, A.A.: Solar eruptions, Forbush decreases, and geomagnetic disturbances from outstanding active region 12673, Space Weather, 16, 1549–1560, doi:10.1029/2018SW001899, 2018.

Christiansen, F.; Papitashvili, V. O.; Neubert, T., Seasonal variations of high-latitude field-aligned currents inferred from Ørsted and Magsat observations, J. Geophys. Res., 107, pp. SMP 5-1, doi:10.1029/2001JA900104, 2002.

Clausen, L. B. N., J. B. H. Baker, J. M. Ruohoniemi, S. E. Milan, J. C. Coxon, S. Wing, S. Ohtani, and B. J. Anderson (2013), Temporal and spatial dynamics of the regions 1 and 2 Birkeland currents during substorms, J. Geophys. Res. Space Physics, 118, 3007–3016, doi:10.1002/jgra.50288.

Clilverd, M.A., Rodger, C.J., Brundell, J.B., Dalzell, M., Martin, I., Mac Manus, D.H., et al.: Long-lasting geomagnetically induced currents and harmonic distortion observed in New Zealand during the 7–8 September 2017 disturbed period, Space Weather, 16, 704-717, doi:10.1029/2018SW001822, 2018.

Coxon, J. C., Milan, S. E., Clausen, L. B. N., Anderson, B. J., & Korth, H. (2014b). A superposed epoch analysis of the regions 1 and 2 Birkeland currents observed by AMPERE during substorms. Journal of Geophysical Research: Space Physics, 119, 9834–9846. https://doi.org/10.1002/2014JA020500.

Cowley, S. W. H. (2000), Magnetosphere-ionosphere interactions: A tutorial review, in Magnetospheric Current Systems, Geophys. Monogr. Ser., vol. 118, pp. 91–106, AGU, Washington, D. C.

Curto, J.J., Marsal, S., Blanch, E., and Altadill, D.: Analysis of the solar flare effects of 6 September 2017 in the ionosphere and in the Earth's magnetic field using spherical elementary current systems, Space Weather, 16, doi:10.1029/2018SW001927, 2018.

Dungey J.W., Interplanetary magnetic fields and the auroral zones. Phys. Rev. Lett. **6**, 47–48 (1961) https://doi.org/10.1103/PhysRevLett.6.47

Dunlop, M. W., Yang, Y.-Y., Yang J.-Y., Lühr, H., Shen, C., et al.: Multispacecraft current estimates at swarm, J. Geophys. Res. Space Phys., 120, doi:10.1002/2015JA021707. 2015.

Elphic, R.C., Bonnell, J.W., Strangeway, R.J., Kepko, L., Ergun, R.E., et al.: The auroral current circuit and field-aligned currents observed by FAST, Geophys. Res. Lett., 25, 2033– 2036, 1998.

Iijima, T., and Potemra T.A.: The amplitude distribution of field-aligned currents at northern high latitudes observed by Triad, J. Geophys. Res., 81(13), 2165–2174, doi:10.1029/JA081i013p02165, 1976.

Iijima, T., Fujii, R., Potemra, T. A., and Saflekos, N. A.: Fieldaligned currents in the south polar cusp and their relationship to the interplanetary magnetic field, J. Geophys. Res., 83, 5595– 5603, doi:10.1029/JA083iA12p05595, 1978.

Iijima, T., Potemra, T. A., Zanetti, L. J., and Bythrow, P. F.: LargeScale Birkeland Currents in the Dayside Polar Region During Strongly Northward IMF: A New Birkeland Current System, J. Geophys. Res., 89, 7441–7452, doi:10.1029/JA089iA09p07441, 1984.

Iijima, T., and Potemra, T.: The amplitude distribution of field-aligned currents associated with substorms, J. Geophys. Res., 83, 599–615, 1978.

Janhunen, P., Olsson, A., Amm, O., and Kauristie, K.: Characteristics of a stable arc based on FAST and MIRACLE observations, Ann. Geophys., 18, 152– 160, 2000.

Johnson, M.L., Murphree, J.S., Marklund, G.T., and Karlsson, T.: Progress on relating optical auroral forms and electric field patterns, J. Geophys. Res., 103, 4271–4284, doi:10.1029/ 97JA00854, 1998.

Juusola, L., Kauristie, K., Vanhamaki, H., Aikio, A., and van de Kamp M.: Comparison of auroral ionospheric and field-aligned currents derived from Swarm and ground magnetic field measurements, J. Geophys. Res. Space Phys., 121, 9256–9283, doi:10.1002/2016JA022961, 2016.

Friis-Christensen, E., Luhr, H., Knudsen, D., and Haagmans, R., Swarm—An Earth observation mission investigating geospace, Adv. Space Res., 2008, vol. 41, no. 1, pp. 210–216.

Fukunishi, H., Fujii, R., Kokubun, S., Tohyama, F., Mukai T., and Oya H.: Small-scale field-aligned currents observed by the Akebono (EXOS-D) satellite, Geophys. Res. Lett., doi:10.1029/91GL00036, 1991.

He, M., Vogt, J. Lühr, H., and Sorbalo, E.: Local time resolved dynamics of field-aligned currents and their response to solar wind variability, J. Geophys. Res. Space Phys., 119, 5305–5315, doi:10.1002/2014JA019776, 2014.

Ganushkina N. Y., M. W. Liemohn , S. Dubyagin , I. A. Daglis , I. Dandouras et al. Defining and resolving current systems in geospace Ann. Geophys., 33, 1369–1402, 2015 www.ann-geophys.net/33/1369/2015/ doi:10.5194/angeo-33-1369-2015

Gjerloev, J.W., S. Ohtani, T. Iijima, B. Anderson, J. Slavin, and G. Le Characteristics of the terrestrial field-aligned current system Ann. Geophys., 29, 1713–1729, 2011 doi:10.5194/angeo-29-1713-2011

Green, D.L., Waters, C.L., Anderson, B.J., and Korth, H.: Seasonal and interplanetary magnetic field dependence of the field-aligned currents for both Northern and Southern Hemispheres, Ann. Geophys., 27, 1701–1715, www.ann-geophys.net/27/1701/2009/, 2009.

Knudsen, D., Burchill, J.K., Berg, K., et al., A low energy charged particle distribution imager with a compact sensor for space applications, Rev. Sci. Instrum., 2003, vol. 74, pp. 202–211.

Korth, H., Anderson, B. J., and Waters, C. L.: Statistical analysis of the dependence of large-scale Birkeland currents on solar wind parameters, Ann. Geophys., 28, pp. 515-530, doi:10.5194/angeo-28-515-2010, 2010.

Laundal, K. M., & Richmond, A. D. (2017). Magnetic coordinate systems. Space Science Reviews, 206, 27–59. https://doi.org/10.1007/s11214-016-0275-y

Lewis, R.V., Williams, P.J.S., Jones, G.O., Opgenoorth, H.J., and Persson, M.A.L.: The electrodynamics of a drifting auroral arc, Ann. Geophys., 12, 478, 1994.

Liemohn, M.W., et al., 2001. Dominant role of the asymmetric ring current in producing the storm-time Dst. Journal of Geophysical Research 106, 10883–10904.Lui, A.T.Y.: Current disruption in the Earth's magnetosphere: Observations and models, J. Geophys. Res., 101, 13 067–13 088, 1996.

Luhr, H., Park, J., Gjerloev, J.W., Rauberg, J., Michaelis, I., Merayo, J.M.G., and Brauer, P.: Field-aligned currents' scale analysis performed with the Swarm constellation. Geophys. Res. Lett., 42, 1–8, doi:10.1002/2014GL062453, 2015.

Lukianova, R., and Kozlovsky, A.: Dynamics of polar boundary of the auroral oval derived from the IMAGE satellite data, Cosmic Res., 51(1), 46–53, 2013.

Lyons, L.R.: Formation of auroral arcs via magnetosphere-ionosphere coupling, Rev. Geophys., 30, 93–112, 1992.

Marchaudon, A., J.-C. Cerisier, R. A. Greenwald, and G. J. Sofko, Electrodynamics of a flux transfer event: Experimental test of the Southwood model, Geophys. Res. Lett., **31**, L09809, doi:10.1029/2004GL019922, 2004.

Marchaudon, A., Cerisier, J.-C., Bosqued, J.-M., Owen, C. J., Fazakerley, A. N., and Lahiff, A. D.: On the structure of field-aligned currents in the mid-altitude cusp, Ann. Geophys., **24**, pp. 3391-3401, doi:10.5194/angeo-24-3391-2006, 2006.

Marklund, G., Sandahl, I., and Opgenoorth, H.: A study of the dynamics of a discrete auroral arc, Planet. Space Sci., 30, 179–197, doi:10.1016/0032-0633(82)90088-5, 1982.

McGranaghan, R.M., Mannucci, A.J., and Forsyth, C.: A comprehensive analysis of multiscale field-aligned currents: Characteristics, controlling parameters, and relationships, J. Geophys. Res.: Space Phys., 122, 11931–11960, doi:10.1002/2017JA024742, 2017.

Merayo, J. G. M., J. L. Jɯrgensen, E. Friis-Christensen, P. Brauer, F. Primdahl, P. S. Jɯrgensen, T. H. Allin, and T. Denver (2008), The Swarm Magnetometry Package, pp. 143–151, Springer, Dordrecht, Netherlands, doi:10.1007/978-1-4020-6943-7_13.

Milan, S.E., Cowley, W.H., Lester, M., Wright, D.M., Slavin, J.A., Fillingim, M., Carlson, C. W., and Singer, H.J.: Response of the magnetotail to changes in the open flux content of the magnetosphere, J. Geophys. Res., 109, doi:10.1029/2003JA010350, 2004.

Neubert, T., and Christiansen, F.: Small-scale, field-aligned currents at the top-side ionosphere, Geophys. Res. Lett., 30(19), 2010, doi:10.1029/2003GL017808, 2003.

Opgenoorth, H.J., Haggstrom, I., Williams, P.J.S., and Jones, G.O.L.: Regions of strongly enhanced perpendicular electric fields adjacent to auroral arcs, J. Atmos. Terr. Phys., 52, 449– 458, doi:10.1016/0021-9169(90)90044-N, 1990.

Papitashvili, V.O., Christiansen, F., and Neubert, T.: A new model of field-aligned currents derived from high-precision satellite magnetic field data, Geophys. Res. Lett., 29(14), 1683, doi:10.1029/2001GL014207, 2002.

Ritter; P., Lühr, H.: Curl-B technique applied to Swarm constellation for determining field-aligned currents, Earth Planets Space, 58(4), 463-476, 2006.

Pu, Z. Y., J. Raeder, J. Zhong, Y. V. Bogdanova, M. Dunlop, C. J. Xiao, X. G. Wang, and A. Fazakerley, Magnetic topologies of an in vivo FTE observed by Double Star/TC-1 at Earth's magnetopause, Geophys. Res. Lett., **40**, pp. 3502–3506, doi:10.1002/grl.50714, 2013.

Ridley A.J., Effects of seasonal changes in the ionospheric conductances on magnetospheric field-aligned currents. Geophys. Res. Lett. **34**, L05101 (2007).

Ritter, P. and Lühr, H.: Near-Earth magnetic signature of magnetospheric substorms and an improved substorm current model, Ann. Geophys., 26, 2781-2793, https://doi.org/10.5194/angeo-26-2781-2008, 2008.

Ritter, P.; Lühr, H.; Rauberg, J., Determining field-aligned currents with the Swarm constellation mission, Earth, Planets and Space, **65**, pp. 1285-1294, doi: 10.5047/eps.2013.09.006, 2013.

Swarm Level 2 Processing System Consortium. Detailed Processing Model (DPM) FAC (Tech. Rep. SW-DS-GFZ-GS-0002): Swarm Level 2 Processing System, 2012.

Southwood, D.J., The ionospheric signature of flux transfer events, J. Geophys. Res., **92**, pp. 3207-3213, 1987.

Tanskanen, E.I.: A comprehensive high-throughput analysis of substorms observed by IMAGE magnetometer network: Years 1993-2003 examined, J. Geophys. Res., 114, A05204, doi:10.1029/2008JA013682, 2009.

Wang, H., Luhr, H., Ma, S.Y., Weygand, J., Skoug, R.M., and Yin, F.: Field-aligned currents observed by CHAMP during the intense 2003 geomagnetic storm events, Ann. Geophys., 24, 311–324, SRef-ID:1432-0576/ag/2006-24-311, 2006.

Weimer, D.R.: Maps of ionospheric field-aligned currents as a function of the interplanetary magnetic field derived from Dynamics Explorer 2 data, J. Geophys. Res., 106, 2889-12902, 2001.

Wu, J., Knudsen, D.J., Gillies, D.M., Donovan, E.F., and Burchill, J.K.: Swarm Observation of Field-Aligned Currents Associated With Multiple Auroral Arc Systems, J. Geophys. Res.: Space Phys., 122, 10145–10156, doi:10.1002/2017JA024439, 2017.

Yasyukevich, Yu., Astafyeva, E., Padokhin, A., Ivanova, V., Syrovatskii, S., and Podlesnyi A.: The 6 September 2017 X-class solar flares and their impacts on the ionosphere, GNSS and HF radio wave propagation, Space Weather, 16, doi:10.1029/2018SW001932, 2018.